energies

MDPI

Article

Dynamic Control of Traction Motor for EV Fed via Dual Source Inverter with a Two Battery System

Siddhant Gudhe [1], Sanjeev Singh [1], Miloud Rezkallah [2,*] and Ambrish Chandra [3]

[1] EED, Maulana Azad National Institute of Technology, Bhopal 462003, India
[2] Research and Innovation Center of Intelligent Energy Management, Sept-Îles, QC G4R 5B7, Canada
[3] Electrical Engineering Department, École de Technologie Supérieure, Montreal, QC H3C 1K3, Canada
* Correspondence: miloud.rezkallah@itmi.ca

Abstract: An electric vehicle uses multiple energy-storage systems to power the traction motor. Dual-source inverters (DSIs) are used for single-stage power conversion by skipping the dc/dc boost converter stage; therefore, eliminating the passive magnetic storing element which improves the overall efficiency of the drive; moreover, multiple energy-storage systems improve the power density of the system. This article discusses the fine control of a traction motor from zero speed to rated speed supplied through a dual-source inverter. Field-oriented control with space vector modulation technique is applied to achieve closed-loop control. Two dc sources are used, one having a higher-voltage battery and one a lower-voltage battery. The higher-voltage battery is the main battery which supplies power to the traction motor, whereas the lower-voltage battery supplies power to supplementary loads of the EV. This article presents improved dynamic behaviour of an induction-motor-driven EV fed from a dual-source inverter using modified closed-loop field-oriented control with space vector modulation. The improvement includes reduced control complexity due to space vector modulation and achieving the option of EV operation in an emergent situation using the same converter and control system. The simulated performance of the presented system is obtained in MATLAB/Simulink. A step-down experimental prototype is used for verification of effective control of the induction motor as the EV is under constant torque variable speed operation with real-time parameters such as power, power factor, current harmonics, and voltage/current stresses across the switch using two batteries individually.

Keywords: battery; electric vehicle; field-oriented control-space vector modulation; dual-source inverter; multi-energy storage system

Citation: Gudhe, S.; Singh, S.; Rezkallah, M.; Chandra, A. Dynamic Control of Traction Motor for EV Fed via Dual Source Inverter with a Two Battery System. *Energies* **2023**, *16*, 1754. https://doi.org/10.3390/en16041754

Academic Editor: Chunhua Liu

Received: 14 January 2023
Revised: 6 February 2023
Accepted: 7 February 2023
Published: 9 February 2023

1. Introduction

Vehicles with an internal combustion (IC) engine significantly contribute to greenhouse gas emissions; thus, the earth's surface temperature has increased tremendously in the last few decades [1]. To tackle this issue, electric vehicles (EVs) are suitable replacements for IC engine vehicles [2]. The primary classification of EVs is hybrid (HEV) and battery-operated (BEV). EVs have rechargeable energy sources such as lead–acid and lithium-ion batteries [3]. Other energy sources, such as hydrogen fuel cells and ultra-capacitors, offer additional merits and take up minimum space compared to the battery packs [4,5] but the high cost of hydrogen fuel cells and ultra-capacitors is still a hurdle for the practical implementation of these sources commercially.

The battery pack supplies power to the traction motor of the EV through power electronics converters. There are multiple converters connecting a battery and the traction motor. In hybrid EVs, the combination of an IC engine and electric motor reduces the need for converters, but the overall complexity of the converter also increases. On the other hand, a traction motor consisting of electrical machines supplied through a power electronics converter delivers higher efficiency and reduced fuel consumption compared

to IC engine vehicles [6–8]. The critical aspects of battery-operated EVs are higher power density, improved efficiency, and cost-effectiveness.

The continuous increase in the power requirement of an EV has resulted in the application of higher-voltage batteries, increasing the driving range of a single charging [9–12]. Three-level neutral point clamped converters are used as inverters to supply power to the traction motor [13–18]; still, voltage balancing is of significant concern and, therefore, gives rise to complex algorithms [13–18]. For example, if a two-level converter operates at high voltage, it shall increase switch voltage stress and have higher power loss. In addition, there is an increase in each switch's blocking voltage, which contributes to additional switching losses; furthermore, a higher load at these converters causes a constant high current through the switches and needs a parallel connection of the switches, but such a configuration increases the conduction losses, and the converter's power density reduces drastically. On the other hand, the three-level NPC converters handle high voltages easily, with reduction of the total harmonic distortion (THD) and power losses, but the complex control, and the requirements of a split capacitor and voltage balancing create significant hurdles to using three-level converters. A three-level NPC inverter uses split capacitor and neutral point connection of the upper and lower switches, which introduces problems of voltage balancing between the split capacitors and distorts the output voltage.

This paper uses a modified topology [19] of the three-level NPC converter for EV application. The major modifications are absent, of a split capacitor and neutral point connection. This eliminates the voltage-balancing problem and reduces the distortion of the output voltage. The critical advantage that motivated this modified topology in EV is using two different dc sources; so, the combination of these dc voltages can provide variable power to the traction motor instead of a single constant dc link. The benefits of using two batteries through a multi-source inverter have been studied recently [20–22]. This single-stage converter interconnects two independent energy-storage systems to the motor's stator and supplementary EV loads as per the load demands. The higher-voltage source is the primary source, while the lower-voltage source acts as a supplementary source. The series–parallel connection of these sources is preferred, or each source is used individually [21,22].

Due to the use of a high-voltage battery directly supplying power to the traction motor, there is no requirement for an additional dc/dc boost converter. Reducing conversion stages, thereby improving efficiency, is a vital advantage of multi-source converter topology. The dc/dc converters essentially require magnetic storing of passive elements and high-frequency switches whose rating matches the battery pack; otherwise, it causes the derating of the battery [21,22]. The multi-source inverter eliminates bulky inductors and use of very high frequency for switches, thereby reducing switching losses. Only two sources are employed in this paper—hence the term dual-source inverter (DSI) is being used.

EV manufacturers prefer various electrical machines such as traction motors, switched reluctance motors, permanent magnet synchronous motors, induction motors, etc. Availability at the variable rating, low cost, and simple and magnet-less construction lead to the induction motor being one of the most suitable options for traction application [23–27]; however, fine control of the induction motor and loss of control at very low speed of the induction motor still form a significant problem; but field-oriented control (FOC) makes it possible to have decoupled control of torque and flux such as that in a separately excited dc motor. Space vector modulation (SVM) is an advanced control technique which controls the inverter in digital form. The SVM technique usually controls dual-source inverters [28–34], but the implementation is still complex due to the series–parallel connections of these dc sources. Though the combination of two sources provides a variable dc link, the system becomes so complicated that the response time increases drastically; furthermore, the behaviour of the drive is complex due to the drive's lower inertia, which results in the mechanical time constant becoming almost equal to the electrical time constant [35].

A coordinated control technique for the induction motor solves the issues related to dual-source inverters. This paper uses the main battery to provide power to the traction

motor only and an extra battery to give power to only supplementary loads of the EV. Supplementary loads include power windows, wipers, speakers, etc. Suppose a case arises in running conditions where the main battery is deeply discharged; in that case, the supplementary battery comes into play, and this extra battery supplies full power to the motor, so that the vehicle avoids halting in the middle of the road. There is coordination between two voltage sources regarding which source to use in normal conditions and which to use in emergencies [36].

A study on dual-source inverters with the independent application of two dc voltages is presented in the literature [36–40] but the dynamic performance and analysis are missing in [36]. The dynamic behaviour has been reported in [37,38], but with variable dc-link; the detailed analysis of variable speed on harmonics and switch stress is not available. The variable speed–torque operation of the induction motor using a dual-source inverter with switch voltage and current stress has been presented in [39,40]; still, a detailed experimental analysis of the control technique in real-time conditions is absent. To address these issues, a collaborative control design is discussed and simulated under the MATLAB/Simulink environment, along with an analysis of dynamic performance. The traction motor is supplied power from both the batteries individually to evaluate the performance of the EV. The motor performance is analyzed at the constant load and variable speed conditions, replicating various driving conditions. The performance simulation obtained is verified on a scaled-down laboratory experimental prototype for the proof of concept. The practical results show speed variation's effect on power, power factor, current harmonics, and voltage/current stresses across the switch.

The organization of this article after introduction is as follows. The second section briefly discusses dual-source inverter topology, and the third section shows the control scheme for dual-source inverters applying FOC with space vector modulation technique. The fourth section shows the performance simulation of the proposed system, and the fifth section shows experimental results. Finally, the conclusion is drawn in the sixth section, followed by the references.

The main contribution of the article is as follows:

a. Modelling and simulation of the dual-source inverter at constant load and variable speed indicating dynamic behaviour of an EV using two battery sources individually;
b. Experimental verification using laboratory prototype of a dual-source inverter to demonstrate the smooth dynamic behaviour for the presented control of an induction motor under normal and emergency operating conditions;
c. Experimental result analysis of the dynamic behaviour indicating parameters such as power, power factor, current harmonics, and voltage/current stresses across the switch using both the dc sources individually.

2. Dual-Source Inverter

The topology of a dual-source inverter (DSI) with two battery systems used in this work is shown in Figure 1. A single conversion stage is used, which connects two dc sources to a single ac source; so, power density increases due to using two batteries in the same EV compared to the system with a single battery. Low-frequency switches select the energy-storage combination, either individually or in a series–parallel combination. Insulated gate bipolar transistors (IGBTs) are used in the dual-source inverter architecture [20,21]. The architecture of the DSI and NPC topology of the three-level inverter shows some similarities in design, but the dc sides of both these topologies are different. DSI topology eliminates the requirement of the neutral point.; thus, the capacitors across each dc source are also independent. DSI gives the output as a three-level line voltage irrespective of the switch configuration used.

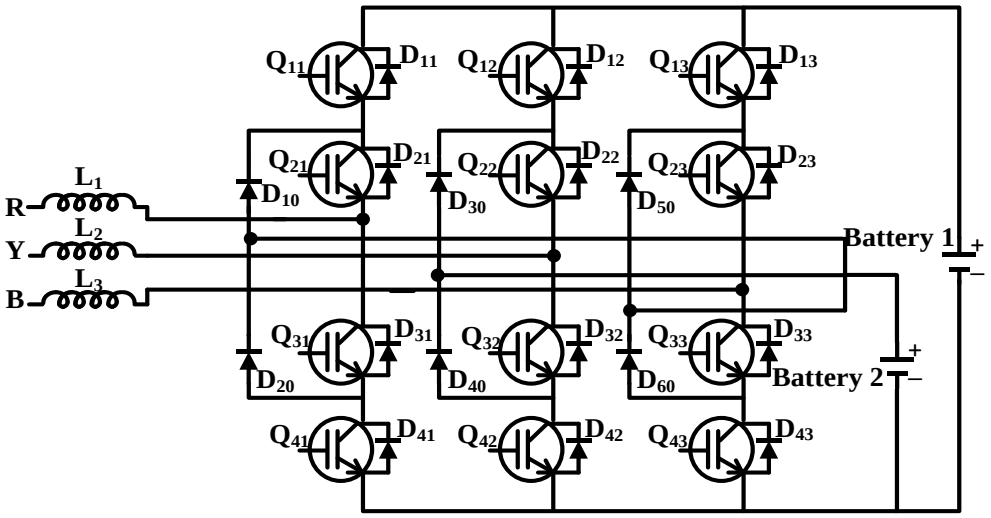

Figure 1. Topology of dual-source inverter [19].

The two simple modes of operation, namely, normal and emergency modes, reduce the control complexity. In the normal mode, power supplied to the traction motor is through the main battery (Batt1), and the auxiliary battery (Batt2) feeds supplementary loads of the EV. In case of emergency, when Batt1 goes into deep discharge during driving, then Batt2 supplies the available power to the traction motor, which is called emergency mode. In emergency mode, the EV motor runs through Batt2, along with only essential supplementary loads such as power windows, headlamps, wipers, etc; however, using Batt2 for a longer duration in emergency mode has disadvantages, as discussed in the next section.

The topology of DSI may use hydrogen fuel cell or ultra-capacitor cells as dc energy sources for EVs; in addition, there may be the use of a combination of ultracapacitor and battery. The ultracapacitor has a faster response time than the battery pack, which means that the battery is used during the running of an EV and the ultracapacitor is used to absorb power during regenerative breaking [6], but different types of energy sources in the single EV complicate the control of the EV, having a massive difference in electrical time constant and mechanical time constant, reducing the system's response time; so, this article recommends the use of two battery systems which are also cost-effective.

3. Control of Dual-Source Inverter

Figure 2 shows the generalized controller which uses the calculation of field angle using rotor position θ_r as an indirect field-oriented control technique. The controller generates phase voltages compared with the carrier signal, which produces signals for switching the dual-source inverter. The current controller has a current loop inside the speed loop. Rotor speed is fed back and compared with the reference speed to give an error signal. The error signal is processed through the PI controller to generate an electromagnetic torque reference signal T_e^*. The same rotor speed creates a flux reference signal ψ_r^*. Below the base speed, the flux maintains a constant value ψ; above the base speed, the flux command signal changes as per equations given in [41], as shown in Figure 2.

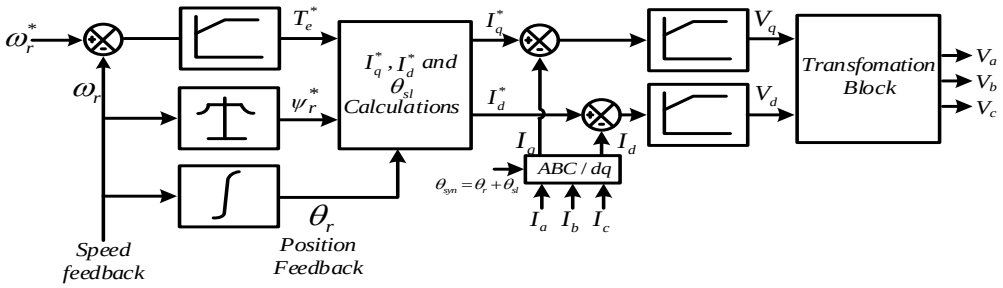

Figure 2. Indirect Field-Oriented Control Scheme.

The rotor position θ_r is the integration of rotor speed which is nothing but the addition of speed at every sample in discrete time. Slip position θ_{sl} is the discrete-time addition of ω_{sl}^*. Synchronous angle θ_{syn} is a simple arithmetic addition of slip angle and rotor angle, which calculates the reference currents I_d and I_q, as shown in Equations (1) and (2). The comparison between the actual and reference currents in the dq-reference frame produces an error, and the error is processed through the PI controller to generate a voltage signal in the dq-reference frame. The command voltages modify the reference three-phase voltages. These reference voltages are compared with the carrier to produce 12 switching signals for the dual-source inverter. All the command signals are always in a synchronous reference frame, which makes signal-processing circuits independent of the requirement of bandwidth [41,42]

The three voltages from the indirect vector control are further processed to control the switching signals of the DSI more precisely by converting voltage signals into reference voltage vector $\overline{V_{ref}}$ and modulating it, which is the space vector modulation technique. $\overline{V_{ref}}$ is the estimation of three-phase reference voltages in the $\alpha\beta$ plane having the magnitude of $\left|\overline{V_{ref}}\right|$ and rotating in an anticlockwise direction, as shown in Figure 3, for both the modes. The magnitude and angle of this voltage vector give two active vectors and one zero vector, and the control scheme is shown in Figure 4. As compared to the neutral point clamped (NPC) topology of the multi-level inverter, only 21 vectors are required for the SVM technique instead of 27 [21,22]. In conventional three-level converters, three switching states ($V_{dc}/2$, 0, and $-V_{dc}/2$) are reflected in each leg's three-phase voltage level, whereas the DSI output voltage synthesis is by three-levels (V_{dc1} or V_{dc2}, 0, and $-V_{dc1}$ or $-V_{dc2}$) of the three switching states in each leg; so, the control becomes simple by controlling speed by a modulation index change with almost similar output.

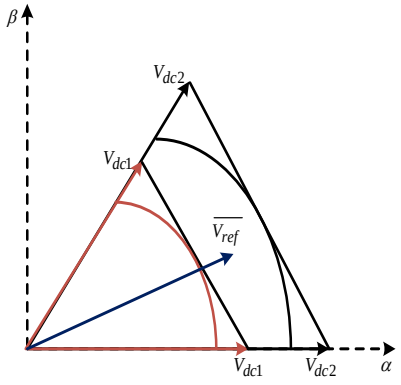

Figure 3. Voltage Space Vector of Proposed modes in sector 1.

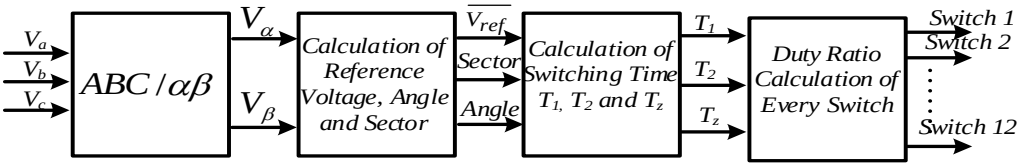

Figure 4. SVM Control Scheme for MSI.

Moreover, this technique has smooth modulation index control according to the load requirement, which was difficult in the indirect field-oriented control technique. The modulation index depends on the dc link voltage and the magnitude of the reference voltage space vector, as indicated in Equations (4) and (5). After selecting the voltage vector magnitude, angle, and the sector in which the voltage vector lies, the time duration T_1, T_2, and T_z determine the duty ratio of each switch, where T_1 and T_2 are the time duration of the nearest two active vectors, and T_z is the time duration of the zero vector.

In both cases, under-modulation and over-modulation control the converter's output voltage. The control is always under modulation when the main battery, V_{dc1}, supplies power. In under-modulation, the control is more precise and accurate. In an emergency case, battery 2 comes into the picture, so as to obtain more magnitude of actual voltage, and the control is around modulation index one ($m = 1$), but the control of output voltage is poor; so, battery 2 (V_{dc2}) is used to run the traction motor only in an emergency case when the voltage level of battery 1 is depleted below the cut-off level. The speed torque characteristics of the motor decrease in mode 2; therefore, at the same motor loading, the maximum speed in mode 2 also decreases.

$$I_d^* = \frac{1}{L_m^*}(\lambda_r^* + \frac{L_r^*}{R_r^*}\frac{d}{dt}\lambda_r^*) \tag{1}$$

$$I_q^* = \frac{4}{3P}\frac{L_r^*}{L_m^*}\frac{T_e^*}{\lambda_r^*} \tag{2}$$

$$\omega_{sl}^* = \frac{R_r^*}{\lambda_r^*}\frac{L_m^*}{L_r^*}I_q^* \tag{3}$$

$$\text{Mode 1} \rightarrow \; m < \frac{\left|\overline{V_{ref}}\right|}{\frac{2}{3}V_{dc1}} \tag{4}$$

$$\text{Mode 2} \rightarrow \; \frac{\left|\overline{V_{ref}}\right|}{\frac{2}{3}V_{dc1}} < m \leq 1. \tag{5}$$

4. Performance Simulation

FOC with SVM technique is applied to control dual-source inverter and modelled in MATLAB/Simulink environment. Two battery sources, 420 V and 200 V, are used, respectively. The rating of the induction motor is 400 V, 33 hp, which directly connects to a 420 V battery. Table 1 gives the detailed specification of the present system. FOC-SVM controls the modulation index, providing smooth induction motor control. The modulation index is directly proportional to the voltage reference vector magnitude and dc voltage as indicated by Equations (4) and (5).

Table 1. Simulation specification.

Parameter	Value
Batt1	420 V Lithium Ion
Batt2	200 V Lead Acid
Power (IM.)	33 HP
Voltage (IM.)	400 V
Rs	0.435 Ω
Ls	4 mH
Rr	0.816 Ω
Lr	2 mH
Inertia	0.09 kg·m^2
Rated Rotor Speed	2000 rpm

Voltage and current from Batt1 to the induction motor at the 0.9 modulation index are shown in Figure 5. The system's dynamic performance is studied when the motor speed increases and decreases. Figures 6 and 7 show the dynamic behaviours indicating current and voltages. Results show a smooth variation of the speed, currents within limits, and a high response time at complete load conditions when Batt1 supplies power to the traction motor. For the concept verification of running the traction motor using an extra battery, the induction motor is supplied directly through the Batt2. Figures 8 and 9 show the voltage and current waveforms, and the currents are within limits with smooth control, but the total power is absorbed by the motor decreases. Due to the low value of the dc voltage, Batt2 has a small modulation index range. An inverse relationship exists between the modulation index and the dc link voltage, as shown in Equations (4) and (5); hence, a decrease in dc voltage increases the modulation index. As a result, the induction motor runs with the best speed–torque characteristics at a modulation index close to 1, and the speed control range decreases; therefore, it is recommended to use Batt2 for emergency conditions only and not for the prolonged running of EVs.

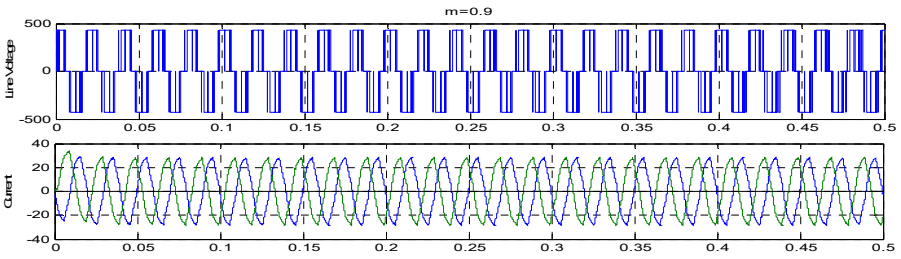

Figure 5. Simulation results of voltage and current at 0.9 modulation index.

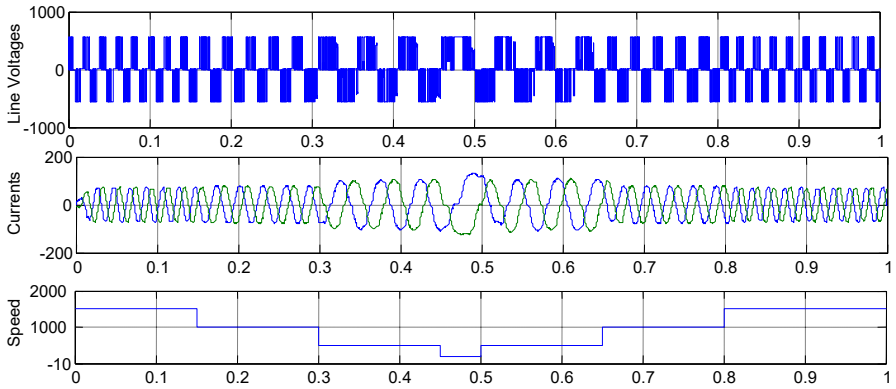

Figure 6. Effect of speed variation (decrement/increment) on voltage and current using the main battery.

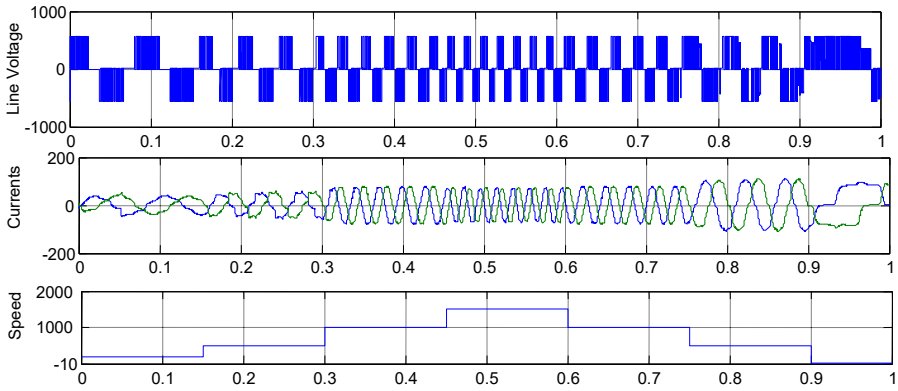

Figure 7. Effect of speed variation (increment/decrement) on voltage and current using the main battery.

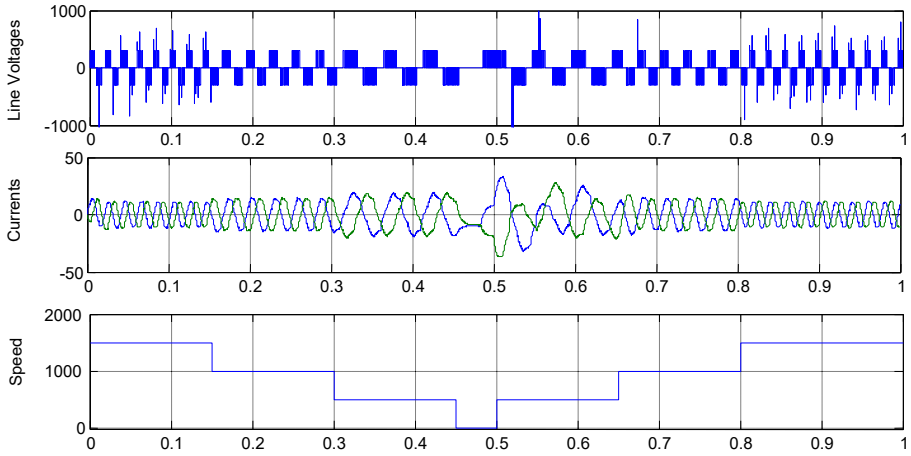

Figure 8. Effect of speed variation (decrement/increment) on voltage and current using the supplementary battery.

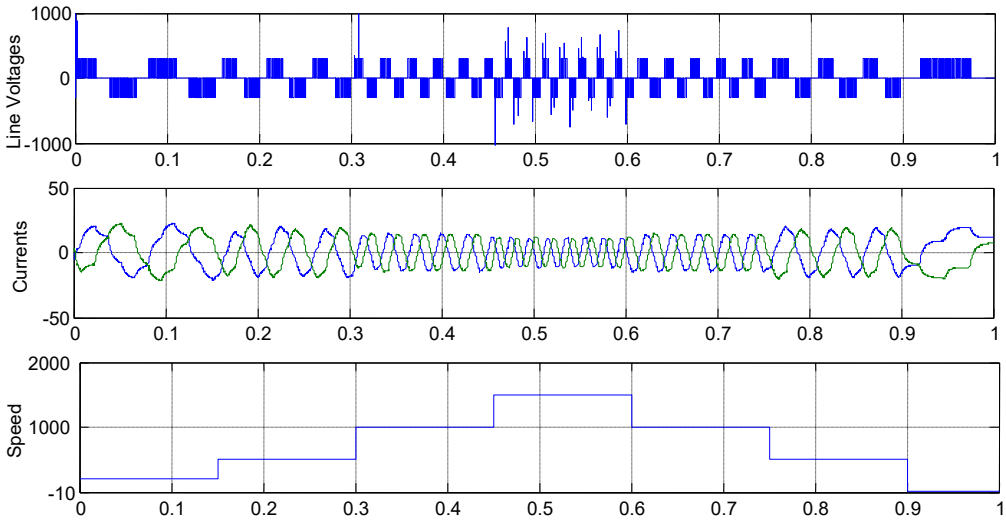

Figure 9. Effect of speed variation (increment/decrement) on voltage and current using the supplementary battery.

5. Experimental Validation

The proposed concept is verified experimentally on a scaled-down laboratory setup which uses a rectifier circuit to create the dc voltage sources at the dc link of the dual-source

inverter. The main dc link voltage is maintained at 450 V, and the supplementary dc link voltage is 300 V. The 450 V dc link voltage provides power to the 415 V, 1 hp induction motor. The induction motor, coupled with a separately excited dc shunt generator of the same rating, acts as a load. The lamp (resistive) load is at the armature terminal of the dc motor running as dc generator, for which the flux is maintained constant in the separately excited winding through the single-phase diode bridge rectifier. A dc tachogenerator is mounted on the motor shaft as speed sensor. The dc signals from the tachogenerator are converted within 5 V dc using a voltage divider circuit, which is fed back to the analog input of the DSP controller. The analog feedback of measured currents through the hall affect sensors in each phase and are given to the DSP controller within limit of 5 V. The induction motor is operated at full load conditions to cause the motor to act the same as an EV traction motor. The modulation index is varied using field-oriented control followed by space vector modulation. The *dSPACE 1104* DSP-based controller provides switching signals to the converter's IGBT switches.

The modulation index changes by varying the reference speed signal ω_r^* through the *ControlDesk* of *dSPACE*, thus controlling the voltage applied to the motor as per the speed demand. The controller gives the switching frequency of 1 kHz for the IGBT switches. There is no requirement for a very high switching frequency as a dc/dc converter is not required at any conversion stage. Table 2 shows the experimental setup specification.

Table 2. Experimental prototype specification.

Parameter	Value
Device for switching	1200 V, 25 A, IGBT IRG4PH50KD
Main source	450 V dc using a bridge rectifier
Supplementary source	300 V dc using a bridge rectifier
controller	dSPACE1104
Sampling time (T_s)	150 µs
Switching frequency	1 kHz
Operating frequency	50 Hz
load	Induction Motor-dc Generator set
Induction motor specification	V_{rms} = 415 V, I_L = 1.75 A, 1410 rpm, star-connected

Figure 10 shows the experimental results for the steady-state voltage and current for the modulation index of 0.9 at constant speed. Figures 11 and 12 show the real-time voltage, current drawn by the battery, and the dc current supplied when the primary source of 450 V and supplementary source of 300 V supply the power. When the dc voltage is across the diode leg of the DSI and the negative terminal, the current drawn by the motor is not purely symmetrical. The reason behind non-sinusoidal currents is that the turn-on time of the diode and IGBTs is small, but the turn-off time of the diode is larger than that of the IGBT; as a result, the reverse recovery of the diode is slow compared to the reverse recovery of IGBT. Such a condition does not occur when the dc voltage is between the positive and negative terminals of the DSI. Figure 13 shows the traction motor's acceleration, cruising, and deceleration when the primary and supplementary sources supply power. During all three conditions, the current and voltage follow the command given by the controller, and values are well within the limits.

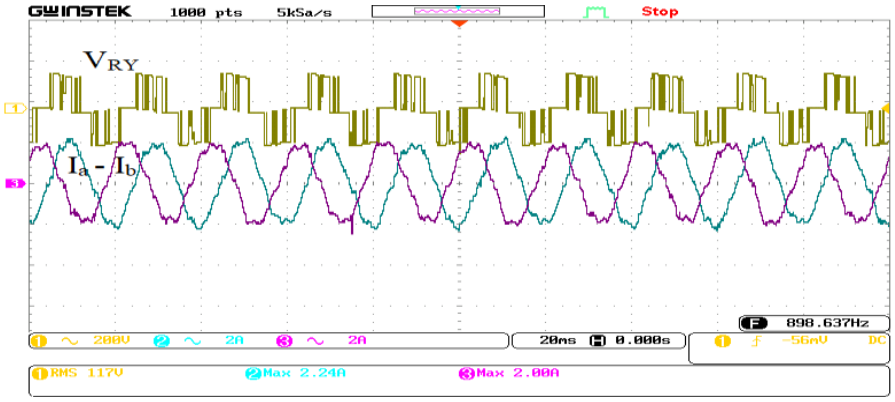

Figure 10. Experimental voltage and current waveform at a modulation index of 0.9.

Figure 11. Experimental voltage, ac input current, and dc output current at low speed and maximum speed when power is supplied through the main source.

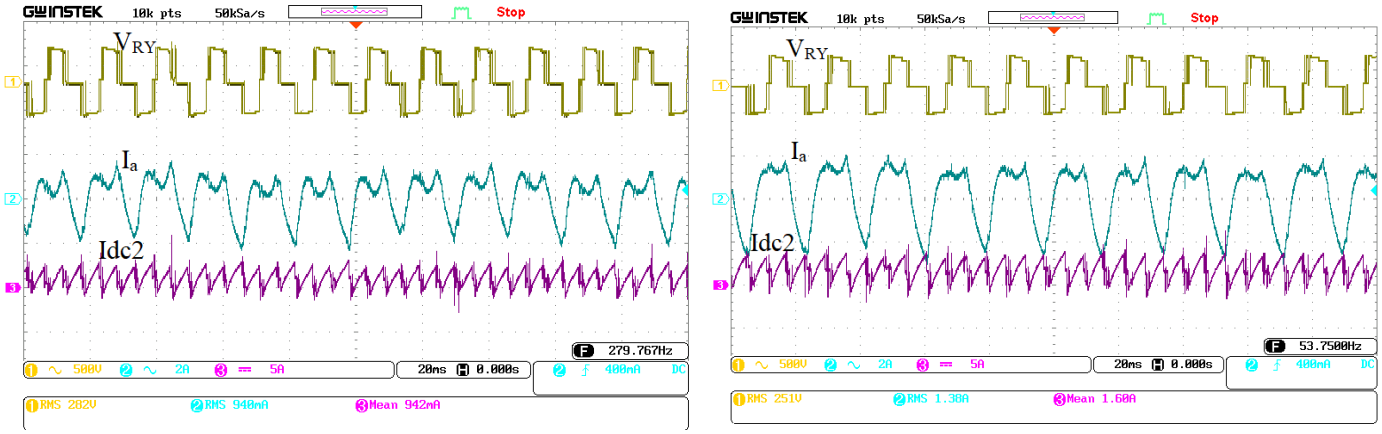

Figure 12. Experimental voltage, ac input current, and dc output current at low speed and maximum speed when power is supplied through the supplementary source.

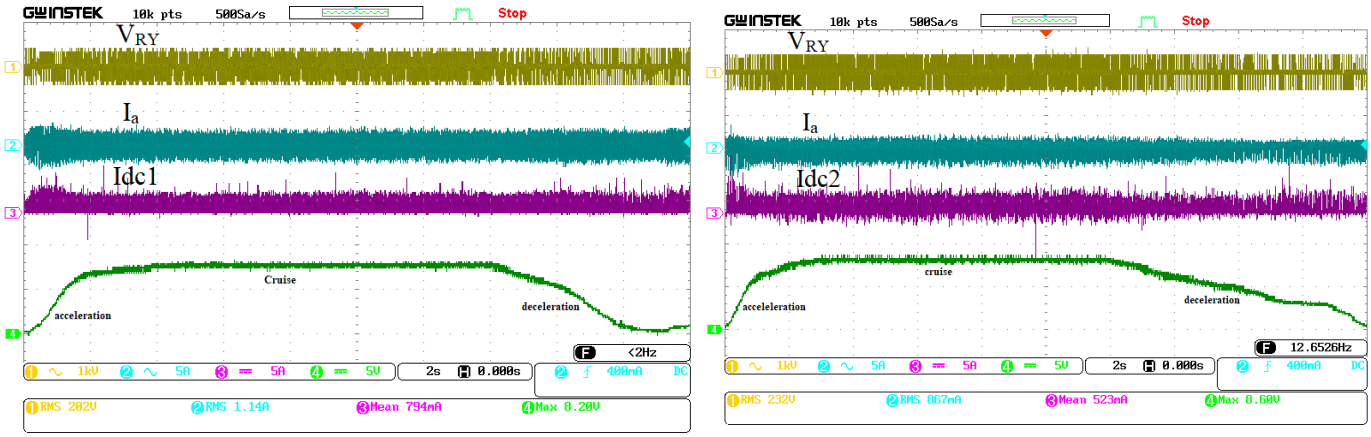

Figure 13. Experimental voltage, ac current, dc current, and speed showing dynamic behavior of the induction motor using the main and the supplementary sources.

To validate the robustness of the controller for real-time conditions, the DSI operates under variable speed conditions. Speed dynamics are verified on an oscilloscope using digital speed through the encoder. It is scaled down in the range of 0 to 10 V, where nearly 8.2 V indicates the rated speed of the motor (nearly 1410 rpm). Due to the limit of the sampling period of the DSP controller (150 µs), some torque ripples are at a lower speed, which can be improved if fast DSP is used. The PI controller inside the control scheme gives a fast response and the modulation index changes as per the speed command outside the current loop. Figure 14a,d show the voltage and current behaviour for a given speed variation when the main battery supplies the power to the induction motor. The variation of speed is achieved through the rotor speed command kept within the range of zero to rated speed in Figure 14a–d. Figure 14d includes the actual rotor speed and rotor reference speed command showing 800 rpm, 1000 rpm, 1300 rpm, and 1400 rpm, approximately, corresponding to the signal at channel 4 of DSO for the tacho-generator output voltage in the range of 5 V, 6 V, 7.5 V, and 8 V, respectively. The voltage output of the tacho-generator is regulated in the range of 0–10 V for depicting the speed of motor as the input to the DSP controller. In contrast, Figure 14e shows the results when the auxiliary battery supplies the power. The current and voltage are within limits from zero to full speed and behave as per command; therefore, a very smooth variation of the induction motor's speed from zero to rated speed is obtained, having constant torque applied during the entire operation. Figure 15 shows a zoomed version of the voltage and current magnitude variation and frequency during speed variation.

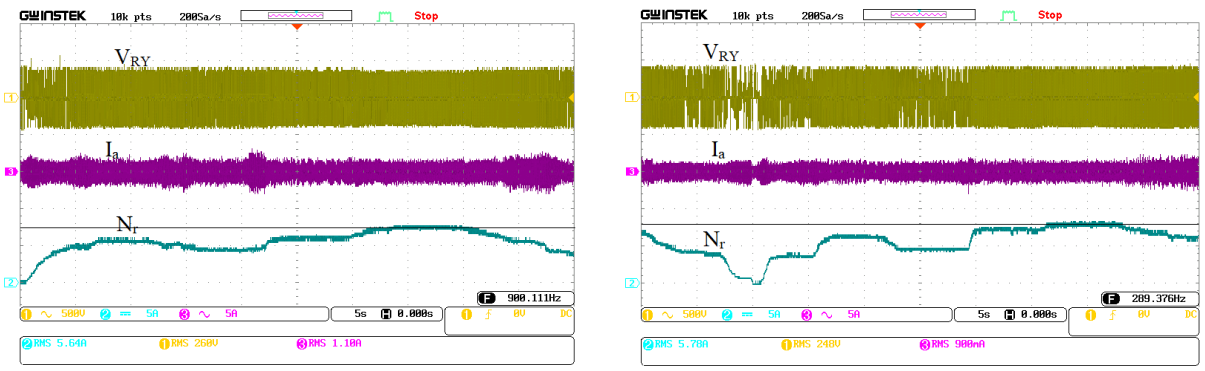

(**a**) (**b**)

Figure 14. *Cont.*

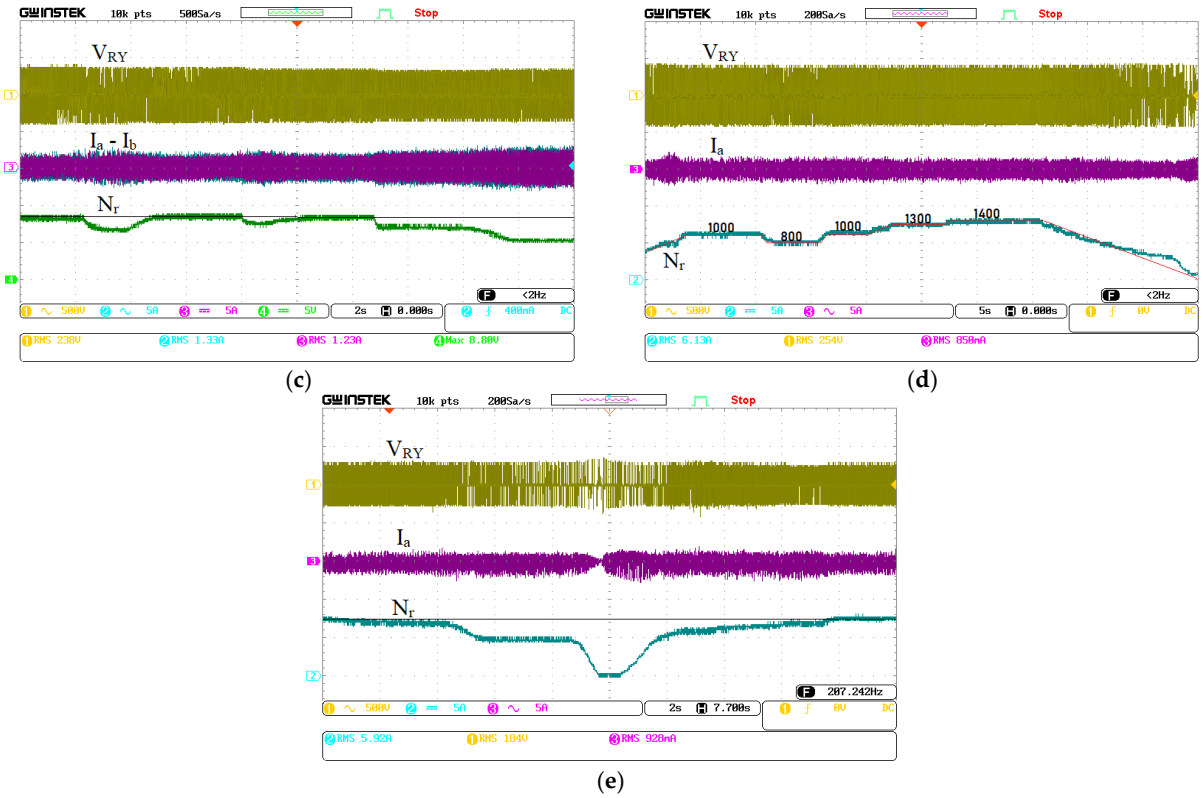

Figure 14. Experimental dynamic behaviors of induction motor supplied through DSI indicating various driving conditions: (**a**–**d**) dc voltage fed from the main source, and (**e**) dc voltage fed from the supplementary source.

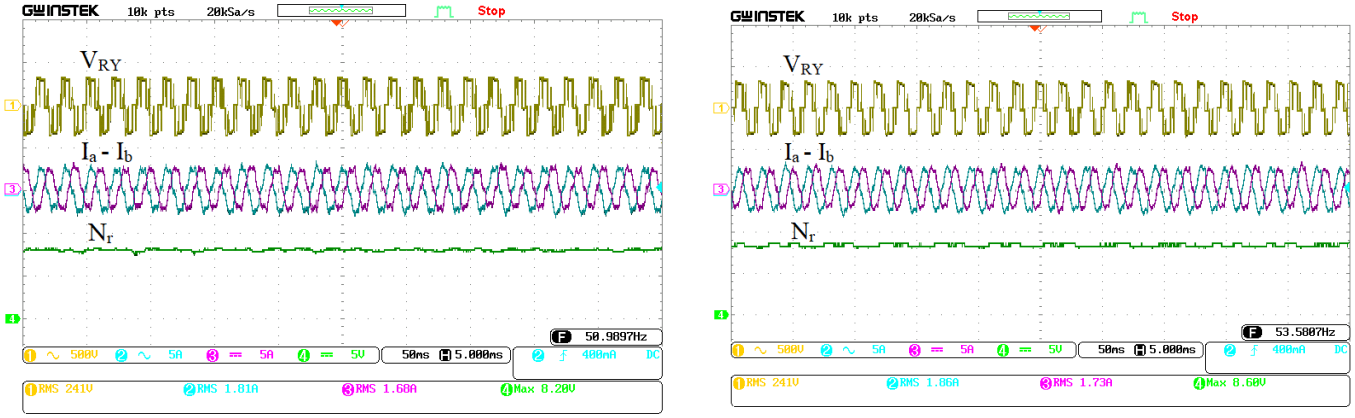

Figure 15. Zoomed waveforms during the variation of speed.

During the steady-state operation of the induction motor from the primary dc source, the current drawn is 1.8 A at the full load conditions for the 1.75 A-rated induction motor. The *Fluke 43B PQ Analyzer* records current harmonics, as shown in Figure 16. The current harmonics are within the prescribed IEEE 519 standard limits of 5%; however, the harmonics vary for the variable speed conditions. These harmonics are recorded at maximum speed and a fully loaded induction motor. Harmonics may increase for the operation of an induction motor at a very low speed; however, the control of the motor is very smooth during very low speed. The reduced harmonics and improved power factor shall finally improve the EV motor's operating efficiency, thereby increasing the EV range.

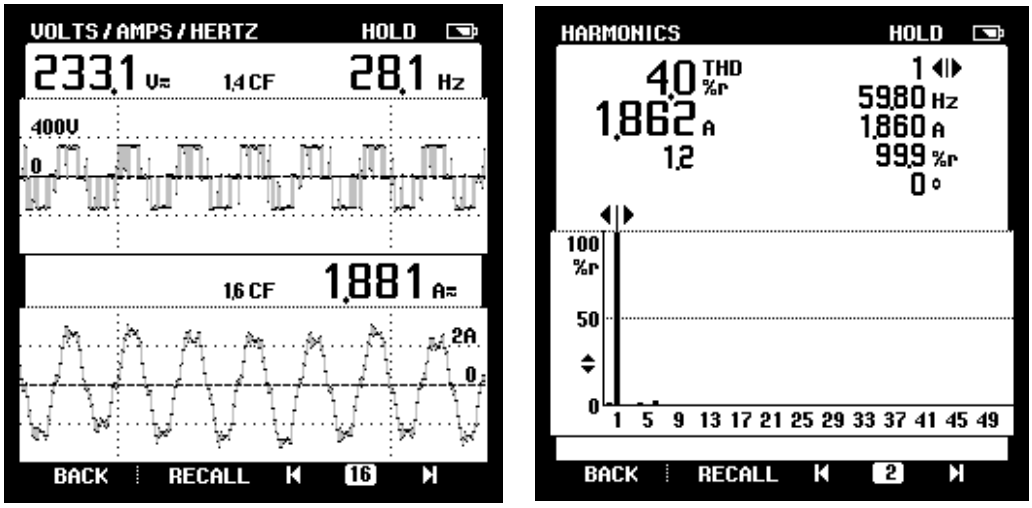

Figure 16. Real-time harmonics of the current waveform.

The controller's real-time robustness is validated, and the effect of speed variation is recorded using a data logger that records power, power factor, voltage, and currents at steady-state conditions. Figure 17 shows the real-time steady state power, power factor, current, and voltage at the complete loaded requirements for the induction motor of 750 W, 1.75 A rating. The current drawn is above the rated value since the motor is operated at lower voltages than the actual voltage rating to provide the power demanded by the load. The data logger also records power, power factor, current, and voltages for nearly 7 min. The real-time graph shows the effect of rapid variation of the speed on this specification. The speed increases from zero, and controllers execute the command to control the speed. Figure 18 shows all the specifications with the range, and a power factor of approximately 0.72 is maintained at almost a constant level since the motor efficiency is 77% at full load on the induction motor; also, the voltage and current are changed proportionally to the power drawn by the motor. These specifications exhibit the same behaviour when the supplementary dc source supplies power, as evidenced in Figure 19. Figure 20 shows the specifications on the nameplate of the induction motor.

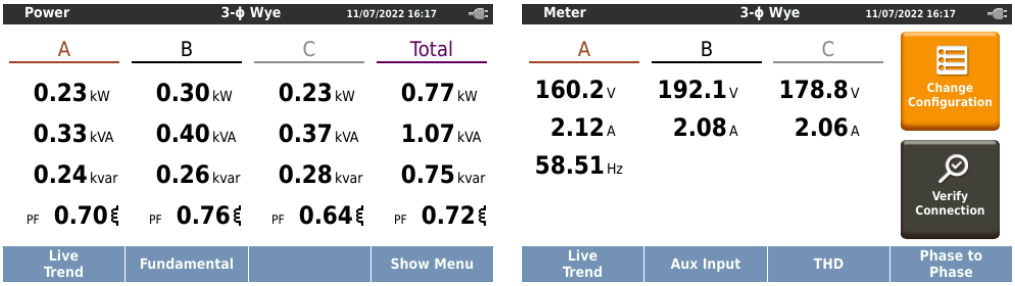

Figure 17. Real-time active power, power factor, voltage, and current using data logger.

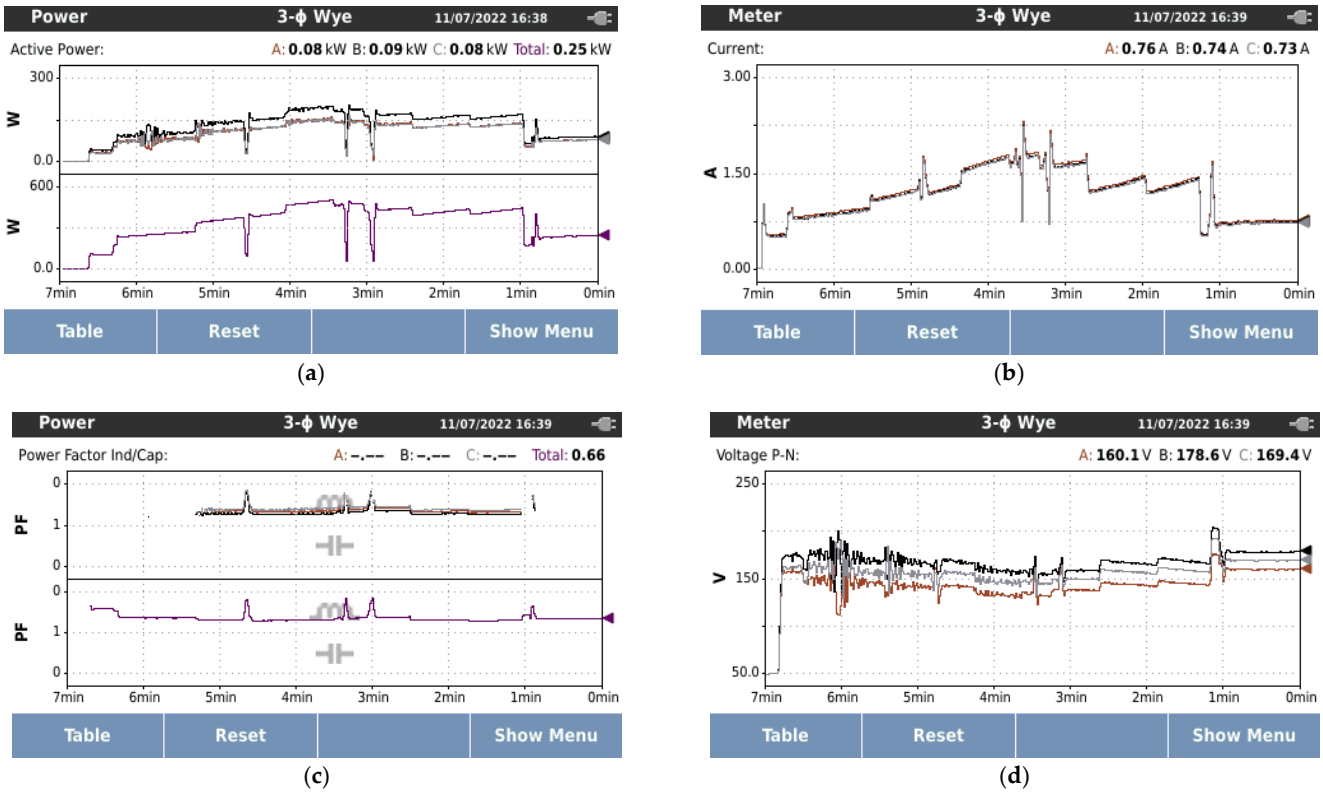

Figure 18. Speed variation effect on (**a**) power, (**b**) current, (**c**) power factor, and (**d**) voltage using the main voltage source.

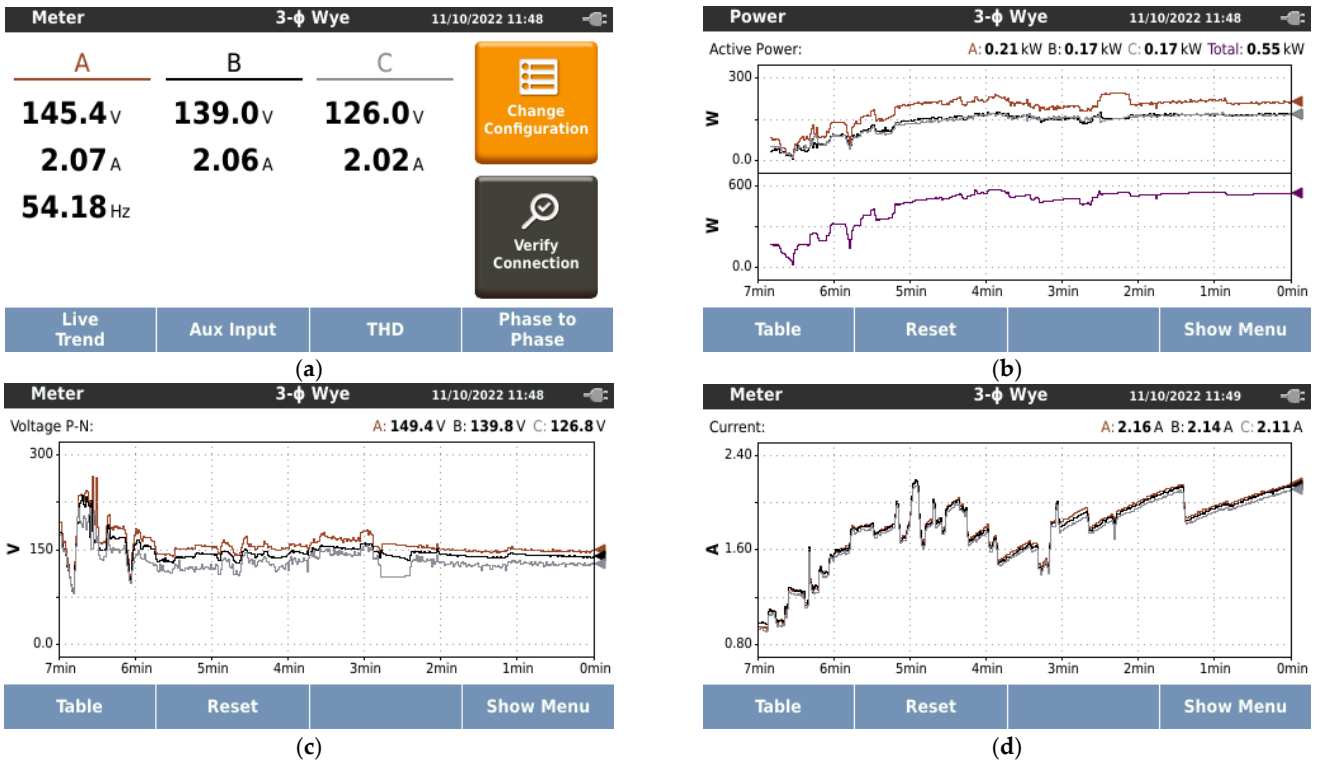

Figure 19. Speed variation effect on (**a**) power, (**b**) current, (**c**) power factor, and (**d**) voltage using the supplementary voltage source.

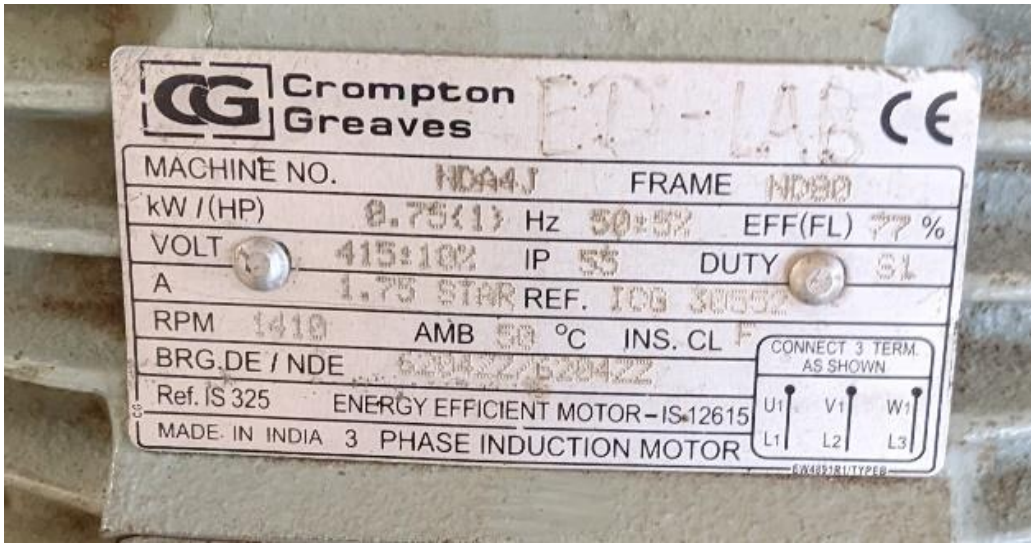

Figure 20. The nameplate of the induction motor used for experimental verification.

Instrument records are presented in terms of voltage and current stress during the running of the induction motor. The data logger records the voltage across the switch and the current through the switch using differential voltage probes and current clamps. It is observed in Figure 21 that the voltage and current do not exceed the switch rating at any given speed. The zoomed voltage and current are shown in Figure 22, indicating steady-state operation.

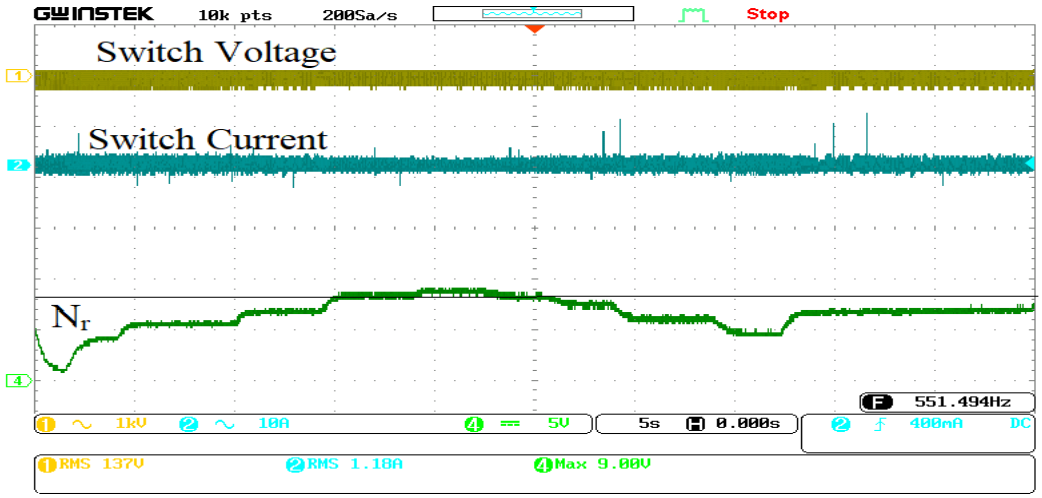

Figure 21. Voltage across switch and current flowing through the switch during variable speed operation.

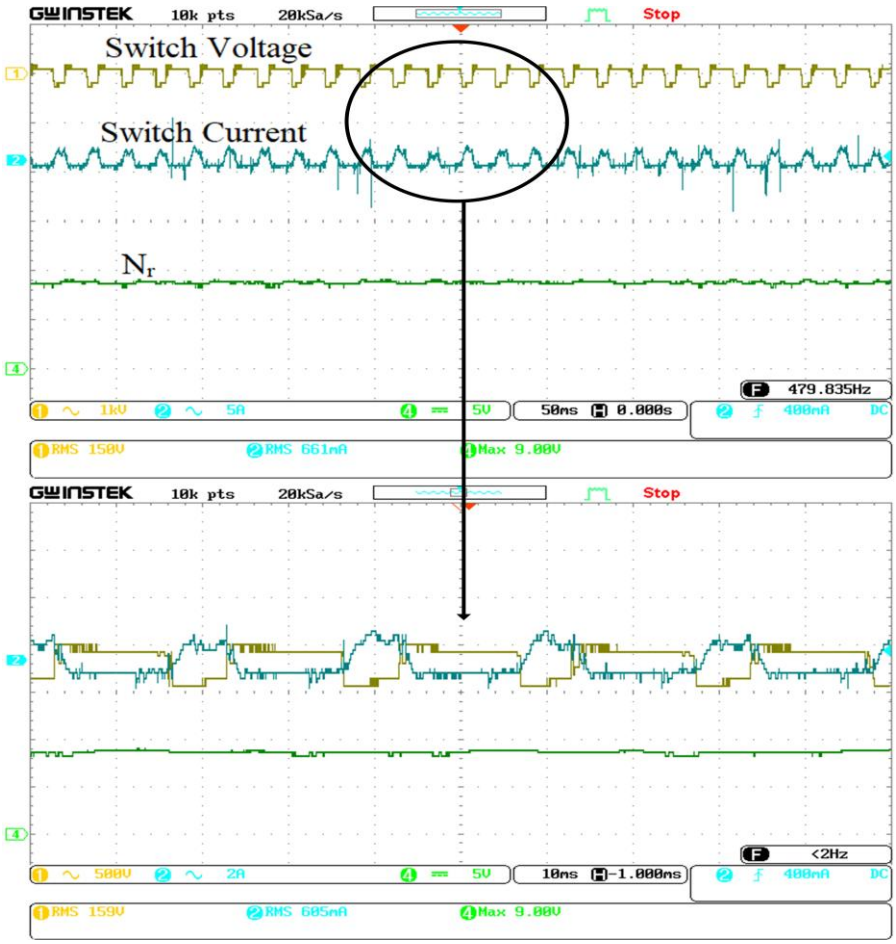

Figure 22. Zoomed voltage across switch and current flowing through switch during variable speed operation.

6. Conclusions

In this paper, dynamic control of a traction motor using a two-battery single-stage converter called a dual-source inverter has been modelled, simulated, and verified experimentally, indicating dynamic behaviour for electric vehicle applications. Field-oriented control with a space vector modulation scheme has been applied through the controller for the induction motor, which acts as a traction motor for EV application consisting of two batteries. A MATLAB/Simulink environment has been used to perform an entirely closed-loop system performance simulation. A scaled-down prototype of 415 V, 1 hp induction motor–dc shunt generator set is employed to validate operating the dc sources individually. A *dSPACE 1104* controller generates the switching signals given to the dual-source inverter. The simulation, as well as experimental results, nearly match the dynamic operating conditions. Based on the experimental results, we conclude that improved control and power factor, reduced current harmonics, and voltage/current stresses lead to overall improvement of efficiency for EV operation so that the range of the EV is enhanced for a single charge; also, the smooth speed variation is obtained from zero to base speed at various driving conditions using the dc sources individually. It is expected that this work shall make a way for deployment of induction motors in EVs with improved controllers to enhance the range of EVs per charge.

Author Contributions: Conceptualization and methodology, S.G. and S.S.; software and validation S.G.; formal analysis and investigation, S.G.; resources and data curation, S.S., M.R. and A.C.; writing—original draft preparation, S.G.; writing—review and editing, S.G., S.S., M.R. and A.C.; visualization, S.G. and S.S.; supervision and project administration, S.S. All authors have read and agreed to the published version of the manuscript.

Funding: This research received no external funding.

Data Availability Statement: Data is contained within the article.

Conflicts of Interest: The authors declare no conflict of interest.

References

1. *42 USC 4§7409*; National Primary and Secondary Ambient Air Quality Standards. United States Congress: Washington, DC, USA, 1977.
2. Cazzola, P.; Gorner, M.; Schuitmaker, R.; Maroney, E. *Global EV Outlook 2016*; International Energy Agency: Paris, France, 2016.
3. Song, K.; Wang, X.; Li, F.; Sorrentino, M.; Zheng, B. Pontryagin's minimum principle-based real-time energy management strategy for fuel cell hybrid electric vehicle considering both fuel economy and power source durability. *Energy* **2020**, *205*, 118064. [CrossRef]
4. Fong, Y.C.; Cheng, K.W.E.; Raman, S.R. A Current Allocation Strategy Based Balancing Technique of Voltage Source String in Switch-Ladder Inverter and Its Switched-Capacitor Variety. *IEEE Trans. Energy Convers.* **2020**, *36*, 1081–1089. [CrossRef]
5. Naderi, E.; Bibek, K.C.; Ansari, M.; Asrari, A. Experimental Validation of a Hybrid Storage Framework to Cope With Fluctuating Power of Hybrid Renewable Energy-Based Systems. *IEEE Trans. Energy Convers.* **2021**, *36*, 1991–2001. [CrossRef]
6. Emadi, A.; Williamson, S.; Khaligh, A. Power electronics intensive solutions for advanced electric, hybrid electric, and fuel cell vehicular power systems. *IEEE Trans. Power Electron.* **2006**, *21*, 567–577. [CrossRef]
7. Perreault, D.; Caliskan, V. Automotive Power Generation and Control. *IEEE Trans. Power Electron.* **2004**, *19*, 618–630. [CrossRef]
8. Rajashekara, K. Power electronics applications in electric/hybrid vehicles. In Proceedings of the 29th Annual Conference of the IEEE Industrial Electronics Society, Roanoke, VA, USA, 2–6 November 2003; Volume 3, pp. 3029–3030. [CrossRef]
9. Taha, W.; Nahid-Mobarakeh, B.; Bauman, J. Efficiency Evaluation of 2L and 3L SiC-Based Traction Inverters for 400 V and 800 V Electric Vehicle Powertrains. In Proceedings of the 2021 IEEE Transportation Electrification Conference & Expo (ITEC), Chicago, IL, USA, 21–25 June 2021; pp. 625–632. [CrossRef]
10. Forouzesh, M.; Liu, Y.F.; Sen, P.C. A Reconfigurable Single-Stage Three-Phase Electric Vehicle DC Fast Charger Compatible With Both 400V and 800V Automotive Battery Packs. In Proceedings of the 2022 24th European Conference on Power Electronics and Applications (EPE'22 ECCE Europe), Hanover, Germany, 5–9 September 2022; pp. 1–11.
11. Abbasi, M.; Kanathipan, K.; Lam, J. An Interleaved Bridgeless Single-Stage AC/DC Converter With Stacked Switches Configurations and Soft-Switching Operation for High-Voltage EV Battery Systems. *IEEE Trans. Ind. Appl.* **2022**, *58*, 5533–5545. [CrossRef]
12. Kim, J.-Y.; Lee, B.-S.; Kwon, D.-H.; Lee, D.-W.; Kim, J.-K. Low Voltage Charging Technique for Electric Vehicles With 800 V Battery. *IEEE Trans. Ind. Electron.* **2021**, *69*, 7890–7896. [CrossRef]
13. Choudhury, A.; Pillay, P.; Williamson, S.S. Comparative Analysis Between Two-Level and Three-Level DC/AC Electric Vehicle Traction Inverters Using a Novel DC-Link Voltage Balancing Algorithm. *IEEE J. Emerg. Sel. Top. Power Electron.* **2014**, *2*, 529–540. [CrossRef]
14. Mukherjee, S.; Giri, S.K.; Kundu, S.; Banerjee, S. A Generalized Discontinuous PWM Scheme for Three-Level NPC Traction Inverter With Minimum Switching Loss for Electric Vehicles. *IEEE Trans. Ind. Appl.* **2018**, *55*, 516–528. [CrossRef]
15. Choudhury, A.; Pillay, P. Space Vector Based Capacitor Voltage Balancing for a Three-Level NPC Traction Inverter Drive. *IEEE J. Emerg. Sel. Top. Power Electron.* **2019**, *8*, 1276–1286. [CrossRef]
16. Choudhury, A.; Pillay, P.; Williamson, S.S. A Hybrid PWM-Based DC-Link Voltage Balancing Algorithm for a Three-Level NPC DC/AC Traction Inverter Drive. *IEEE J. Emerg. Sel. Top. Power Electron.* **2015**, *3*, 805–816. [CrossRef]
17. Gao, Z.; Lu, Q. A Hybrid Cascaded Multilevel Converter Based on Three-Level Cells for Battery Energy Management Applied in Electric Vehicles. *IEEE Trans. Power Electron.* **2018**, *34*, 7326–7349. [CrossRef]
18. Mukherjee, S.; Giri, S.K.; Banerjee, S. A Flexible Discontinuous Modulation Scheme With Hybrid Capacitor Voltage Balancing Strategy for Three-Level N.P.C. Traction Inverter. *IEEE Trans. Ind. Electron.* **2019**, *66*, 3333–3343. [CrossRef]
19. Emadi, A.; Magne, P. Power Converter. U.S. Patent 0117770 A1, 1 May 2014.
20. Ebrahimi, J.; Salari, O.; Eren, S.; Hashtrudi-Zaad, K.; Bakhshai, A.; Jain, P. Efficiency Improved Multi-Source Inverter for Hybrid Energy Storage Systems in Electric Vehicle Application. *IEEE Trans. Power Electron.* **2021**, *37*, 1982–1997. [CrossRef]
21. Dorn-Gomba, L.; Magne, P.; Danen, B.; Emadi, A. On the Concept of the Multi-Source Inverter for Hybrid Electric Vehicle Powertrains. *IEEE Trans. Power Electron.* **2017**, *33*, 7376–7386. [CrossRef]
22. Dorn-Gomba, L.; Guo, J.; Emadi, A. Multi-Source Inverter for Power-Split Hybrid Electric Powertrains. *IEEE Trans. Veh. Technol.* **2019**, *68*, 6481–6494. [CrossRef]

23. Wang, T.; Zheng, P.; Zhang, Q.; Cheng, S. Design characteristics of the induction motor used for hybrid electric vehicle. *IEEE Trans. Magn.* **2005**, *41*, 505–508. [CrossRef]
24. Nagataki, M.; Kondo, K.; Yamazaki, O.; Yuki, K.; Nakazawa, Y. Online Auto-Tuning Method in Field-Orientation-Controlled Induction Motor Driving Inertial Load. *IEEE Open J. Ind. Appl.* **2022**, *3*, 125–140. [CrossRef]
25. Muduli, U.R.; Beig, A.R.; Behera, R.K.; Al Jaafari, K.; Alsawalhi, J.Y. Predictive Control With Battery Power Sharing Scheme for Dual Open-End-Winding Induction Motor Based Four-Wheel Drive Electric Vehicle. *IEEE Trans. Ind. Electron.* **2021**, *69*, 5557–5568. [CrossRef]
26. Kousalya, V.; Rai, R.; Singh, B. Sliding Model-Based Predictive Torque Control of Induction Motor for Electric Vehicle. *IEEE Trans. Ind. Appl.* **2021**, *58*, 742–752. [CrossRef]
27. Wang, H.; Yang, Y.; Ge, X.; Zuo, Y.; Yue, Y.; Li, S. PLL- and FLL-Based Speed Estimation Schemes for Speed-Sensorless Control of Induction Motor Drives: Review and New Attempts. *IEEE Trans. Power Electron.* **2021**, *37*, 3334–3356. [CrossRef]
28. Salari, O.; Zaad, K.H.; Bakhshai, A.; Jain, P. Pseudo Multi Level Space Vector Modulation Technique for Multi Source Inverters. In Proceedings of the 2021 IEEE Energy Conversion Congress and Exposition (ECCE), Vancouver, BC, Canada, 10–14 October 2021; pp. 4979–4986.
29. Salari, O.; Zaad, K.H.; Kumar, A.; Bakhshai, A.; Jain, P. On the Concept of Four Nearest Space Vector PWM for Multi Source Inverters. In Proceedings of the 2019 IEEE Energy Conversion Congress and Exposition (ECCE), Baltimore, MD, USA, 29 September–3 October 2019; pp. 1816–1821.
30. Riache, Y.; Hamdi, E.S. A Novel switching pattern of Modified SVPWM for Z-Source Inverter connected to a Multi-Source System. In Proceedings of the 2018 53rd International Universities Power Engineering Conference (UPEC), Glasgow, UK, 4–7 September 2018; pp. 1–5.
31. Salari, O.; Nouri, M.; Zaad, K.H.; Bakhshai, A.; Jain, P. Space Vector Modulation for Multi-Source Inverters. In Proceedings of the 2018 IEEE International Power Electronics and Application Conference and Exposition (PEAC), Shenzhen, China, 4–7 November 2018; pp. 1–6.
32. Luciano, C.; Aganah, K.A.; Ndoye, M.; Oni, B. New Switched-Multi-Source Inverter Topology with Optimum Number of Used Switches. In Proceedings of the 2018 IEEE PES/IAS PowerAfrica, Cape Town, South Africa, 28–29 June 2018; pp. 414–419.
33. Lawan, M.M.G.; Raharijaona, J.; Camara, M.B.; Dakyo, B. Three level Neutral-Point-Clamped Inverter Control Strategy using SVPWM for Multi-Source System Applications. In Proceedings of the 2019 IEEE International Conference on Industrial Technology (ICIT), Melbourne, Australia, 13–15 February 2019; pp. 562–567.
34. Chemali, E.; Emadi, A. On the concept of a novel Reconfigurable Multi-Source Inverter. In Proceedings of the 2017 IEEE Transportation Electrification Conference and Expo (ITEC), Harbin, China, 7–10 August 2017; pp. 707–713.
35. Wildi, T. *Electric Machines, Drives and Power Systems*; Pearson: London, UK, 2022.
36. Gudhe, S.; Singh, S. Co-ordinated Control of Two Batteries for Traction Motor and Auxiliary Loads in Electric Vehicle. In Proceedings of the 2022 IEEE 2nd International Conference on Sustainable Energy and Future Electric Transportation (SeFeT), Hyderabad, India, 4–6 August 2022; pp. 1–6.
37. Fedele, E.; Iannuzzi, D.; Tricoli, P.; Del Pizzo, A. NPC-based Multi-Source Inverters for Multimode DC Rail Traction Systems. *IEEE Trans. Transp. Electrif.* **2022**. Early access. [CrossRef]
38. Salari, O.; Zaad, K.H.; Bakhshai, A.; Jain, P. Reconfigurable Hybrid Energy Storage System for an Electric Vehicle DC–AC Inverter. *IEEE Trans. Power Electron.* **2020**, *35*, 12846–12860. [CrossRef]
39. Gudhe, S.; Singh, S. Single Stage Multiple Source Bidirectional Converter for Electric Vehicles. In *Flexible Electronics for Electric Vehicles*; Lecture Notes in Electrical Engineering; Springer: Singapore, 2022; Volume 852, pp. 567–574.
40. Gudhe, S.; Singh, S. Charging of Multiple Batteries Using Single-Stage Multi-source Converter with Bidirectional Power Flow. In *Recent Advances in Power Electronics and Drives*; Lecture Notes in Electrical Engineering; Springer: Singapore, 2022; Volume 863, pp. 207–216.
41. Krishnan, R. *Electric Motor Drives: Modeling, Analysis, and Control*; Pearson: London, UK, 2005.
42. Durán, M.J.; Prieto, J.; Barrero, F.; Riveros, J.A.; Guzman, H. Space-Vector P.W.M. With Reduced Common-Mode Voltage for Five-Phase Induction Motor Drives. *IEEE Trans. Ind. Electron.* **2013**, *60*, 4159–4168. [CrossRef]